

Convergence for nonconvex ADMM, with applications to CT imaging

Rina Foygel Barber* and Emil Y. Sidky†

March 25, 2022

Abstract

The alternating direction method of multipliers (ADMM) algorithm [Boyd et al., 2011] is a powerful and flexible tool for complex optimization problems of the form $\min\{f(x) + g(y) : Ax + By = c\}$. ADMM exhibits robust empirical performance across a range of challenging settings including nonsmoothness and nonconvexity of the objective functions f and g , and provides a simple and natural approach to the inverse problem of image reconstruction for computed tomography (CT) imaging. From the theoretical point of view, existing results for convergence in the nonconvex setting generally assume smoothness in at least one of the component functions in the objective. In this work, our new theoretical results provide convergence guarantees under a restricted strong convexity assumption without requiring smoothness or differentiability, while still allowing differentiable terms to be treated approximately if needed. We validate these theoretical results empirically, with a simulated example where both f and g are nondifferentiable (and thus outside the scope of existing theory), as well as a simulated CT image reconstruction problem.

1 Introduction

In this work, we consider optimization problems of the form

$$\text{Minimize } f(x) + g(y) \text{ subject to the constraint that } Ax + By = c. \quad (1)$$

Problems of this form arise in many applications throughout the physical and biological sciences. In particular, we are interested in optimization problems pertaining to computed tomography (CT) imaging, which, as we will see later on, can often be expressed in this type of formulation.

Solving the optimization problem (1) can be computationally challenging even when the functions f and g are both convex. Challenges in the convex setting may include high dimensionality of the variables x and y , nondifferentiability of f and/or g , or poor conditioning of

*rina@uchicago.edu ; Department of Statistics, University of Chicago

†sidky@uchicago.edu ; Department of Radiology, University of Chicago

the linear transformations A, B or the functions f, g . If one or both functions are nonconvex, this brings an additional level of difficulty to the optimization problem.

In this work, we study a linearized form of the alternating directions method of multipliers (ADMM) algorithm [Boyd et al., 2011], in the setting where f and g may both be nonconvex and nonsmooth. While variants of this algorithm are very well known in the literature, existing theoretical results have typically been restricted to narrower settings (e.g., assuming that at least one of the two functions f, g must be smooth), and thus cannot be applied to guarantee convergence for many settings arising in modern high dimensional optimization and data analysis.

Outline In Section 2, we describe the nonconvex linearized ADMM algorithm, and review known results in the literature on the convergence properties of this type of algorithm in various settings. In Section 3 we present our new convergence result, which addresses a more flexible setting allowing both f and g to be potentially nonconvex and nonsmooth. We demonstrate the performance of the algorithm on a simple simulated covariance estimation problem in Section 4, and present an application to computed tomography (CT) imaging in Section 5. Finally, some future directions and implications of this work are discussed in Section 6.

2 Setting and background

Consider the optimization problem

$$\text{Minimize } f(x) + g(y) \quad : \quad x \in \mathbb{R}^d, y \in \mathbb{R}^m \text{ such that } Ax + By = c \quad (2)$$

where the functions f on \mathbb{R}^d and g on \mathbb{R}^m are potentially nonconvex and/or nondifferentiable, while $A \in \mathbb{R}^{k \times d}$, $B \in \mathbb{R}^{k \times m}$, and $c \in \mathbb{R}^k$ define linear constraints on the variables. We will assume that we can write

$$f(x) = f_c(x) + f_d(x), \quad g(y) = g_c(y) + g_d(y)$$

where f_c is convex (possibly nondifferentiable) and f_d is differentiable (possibly nonconvex), and similarly for g_c and g_d . This decomposition allows us to take linear approximations to the differentiable terms f_d and g_d , where needed, in order to ensure simple calculations for each update step of our iterative algorithm.

We will assume that f and g are *proper functions*. Formally, this means that we can write

$$f : \mathbb{R}^d \rightarrow \mathbb{R} \cup \{+\infty\},$$

and we assume that $\text{dom}(f) := \{x \in \mathbb{R}^d : f(x) < +\infty\}$ is nonempty (and similarly for g). We will also assume that $\text{dom}(f) \subseteq \mathbb{R}^d$ and $\text{dom}(g) \subseteq \mathbb{R}^m$ are convex sets.

2.1 Background and prior work

2.1.1 ADMM for convex optimization problems

The alternating directions method of multipliers (ADMM) algorithm, studied by Boyd et al. [2011], treats problems of the form (2). It was developed initially for the setting where f and g are both convex, and operates by reformulating the optimization problem (2) with an augmented Lagrangian,

$$\min_{x,y} \max_u \{ \mathcal{L}_\Sigma(x, y, u) \},$$

where the augmented Lagrangian is defined as

$$\mathcal{L}_\Sigma(x, y, u) = f(x) + g(y) + \langle u, Ax + By - c \rangle + \frac{1}{2} \|Ax + By - c\|_\Sigma^2, \quad (3)$$

for some positive definite penalty matrix $\Sigma \succ 0$.

The ADMM algorithm solves this optimization problem as follows: initializing at some x_0, u_0, y_0 , for all $t \geq 0$ we run the steps:

$$\begin{cases} x_{t+1} = \arg \min_x \{ \mathcal{L}_\Sigma(x, y_t, u_t) \}, \\ u_{t+1} = u_t + \Sigma(Ax_{t+1} + By_t - c), \\ y_{t+1} = \arg \min_y \{ \mathcal{L}_\Sigma(x_{t+1}, y, u_{t+1}) \}. \end{cases} \quad (4)$$

Adding step size matrices In some cases, adding step size matrices $H_f \succeq 0$ for the x update and $H_g \succeq 0$ for the y update can improve the convergence behavior and/or may allow for easier calculation of the update steps:

$$\begin{cases} x_{t+1} = \arg \min_x \left\{ \mathcal{L}_\Sigma(x, y_t, u_t) + \frac{1}{2} \|x - x_t\|_{H_f}^2 \right\}, \\ u_{t+1} = u_t + \Sigma(Ax_{t+1} + By_t - c), \\ y_{t+1} = \arg \min_y \left\{ \mathcal{L}_\Sigma(x_{t+1}, y, u_{t+1}) + \frac{1}{2} \|y - y_t\|_{H_g}^2 \right\}. \end{cases} \quad (5)$$

(Here \succeq denotes the positive semidefinite ordering on matrices, i.e., $H_f \succeq 0$ means that H_f is positive semidefinite.)

In many cases, choosing H_f so that $D_f := H_f + A^\top \Sigma A$ is diagonal, or is a multiple of the identity, may be convenient for calculating the x update step—this is because the x update step is a minimization problem of the form $\arg \min_x \{ f(x) + \frac{1}{2} x^\top D_f x - x^\top v_t \}$, where v_t is a vector that depends on the previous iteration. Specifically, this type of choice for H_f can be helpful when the function f separates over the coefficients of x , $f(x) = \sum_i f_i(x_i)$ (so that now, the x update step separates completely over the coefficients of x).

Another setting where this type of modification is commonly used is when f is equipped with an inexpensive proximal map (the map $z \mapsto \arg \min \{ f(x) + \frac{1}{2} \|x - z\|_2^2 \}$)—for example, the ℓ_1 norm, $f(x) = \|x\|_1$, or the ℓ_2 norm, $f(x) = \|x\|_2$, are both commonly used regularization functions that have simple proximal maps. (Without the matrix H_f , the x update step is of the form $\arg \min_x \{ f(x) + \frac{1}{2} x^\top A^\top \Sigma A x - x^\top v_t \}$, which may be substantially more challenging

to compute if $A^\top \Sigma A$ is a dense matrix.) Similarly we may choose H_g with these types of considerations in mind for the y update step.

This type of modification of ADMM is often referred to as *linearization*, and is closely linked to related algorithms for composite optimization problems of the form $f(Ax) + g(x)$, studied via primal-dual methods by, e.g., Chen and Teboulle [1994], Chambolle and Pock [2011], He and Yuan [2012], Valkonen [2014], among many others, and has been applied to convex versions of the CT image reconstruction problem (see, e.g., Nien and Fessler [2014]).

Linear approximations For many optimization problems, even with the modification of a step size matrix (i.e., linearization), it may still be challenging to compute the x update step if the function f is difficult to minimize (and similarly, the y step with the function g). In particular, if the x update step itself can only be solved with an iterative procedure, this type of “inner loop” will drastically slow down the convergence of ADMM.

An alternative is to replace the function f with an approximation at each step. In particular, consider our earlier decomposition, $f = f_c + f_d$, where f_c is convex while f_d is differentiable. We will take a linear approximation to f_d (note that this is not to be confused with the term “linearization”, which is used to describe modifications to how we handle the Lagrangian term $\frac{1}{2}\|Ax + By - c\|_\Sigma^2$, as described above.)

At the current iteration x_t , we can approximate the function f as

$$f(x) \approx f_c(x) + (f_d(x_t) + \langle \nabla f_d(x_t), x - x_t \rangle).$$

Although this inexact calculation of the x update may lead to slower convergence in terms of the total number of iterations, this may be outweighed if this approximation allows the cost of each single iteration to be substantially reduced. We can make the analogous modification for the y update step. This type of modification has been commonly used in both the convex and nonconvex settings (see below for references in the nonconvex setting).

For completeness, Algorithm 1 presents this modified form of ADMM (combining both linear approximations to f_d and g_d , and the “linearization” via step size matrices described above). This is the version of the algorithm that we will study in our work.

2.1.2 Nonconvex ADMM

Next we turn to the nonconvex setting, where the functions f and/or g are no longer required to be convex. In many optimization problems, the ADMM algorithm (possibly with the addition of step size matrices H_f, H_g and/or linear approximations to f_d, g_d) has been observed to perform well, converging successfully and avoiding issues such as saddle points or local minima. The convergence properties in a nonconvex setting have been studied extensively. For example, Wang et al. [2014], Hong et al. [2016], Magnússon et al. [2015], Wang et al. [2019] study the performance of ADMM with f and g update steps calculated exactly (with Wang et al. [2018] extending the algorithm to handle more than two variable blocks), while Mukkamala et al. [2019], Jiang et al. [2019], Lanza et al. [2017] study the algorithm with linear approximations to (parts of) f and/or g . All of these works prove results of one of the two following types:

Algorithm 1 ADMM with linear approximations

Input: Functions $f = f_c + f_d$ and $g = g_c + g_d$, with f_c, g_c convex, f_d, g_d differentiable; matrices A, B ; vector c ; penalty matrix $\Sigma \succ 0$; step size matrices $H_f, H_g \succeq 0$.

Initialize: x_0, y_0, u_0 .

for $t = 0, 1, 2, \dots$ **do**

$$\begin{aligned} \text{Update } x: \quad x_{t+1} = \arg \min_x \left\{ f_c(x) + \frac{1}{2} \|x - x_t\|_{H_f + A^\top \Sigma A}^2 \right. \\ \left. + \langle x, \nabla f_d(x_t) + A^\top \Sigma (Ax_t + By_t - c) + A^\top u_t \rangle \right\}. \end{aligned}$$

$$\text{Update } u: \quad u_{t+1} = u_t + \Sigma (Ax_{t+1} + By_t - c).$$

$$\begin{aligned} \text{Update } y: \quad y_{t+1} = \arg \min_y \left\{ g_c(y) + \frac{1}{2} \|y - y_t\|_{H_g + B^\top \Sigma B}^2 \right. \\ \left. + \langle y, \nabla g_d(y_t) + B^\top \Sigma (Ax_{t+1} + By_t - c) + B^\top u_{t+1} \rangle \right\}. \end{aligned}$$

until some convergence criterion is reached.

- Assume that either f or g is differentiable and has a Lipschitz gradient, and establish convergence guarantees;
- Assume that the algorithm converges (or, more weakly, assume only that the dual variable u_t converges), and establish optimality properties of the limit point.

It is important to note that neither type of existing result verifies that convergence is guaranteed in the setting where both f and g are nondifferentiable.

A different type of nonconvexity that is studied in the literature is where f and g are both convex, but the constraint on (x, y) is nonconvex (e.g., $y = A(x)$ for a nonlinear operator A); this type of problem is studied by Valkonen [2014], Ochs et al. [2015], among others.

2.1.3 The MOCCA algorithm

Our own earlier work on this problem [Barber and Sidky, 2016] proposed the Mirrored Convex/Concave algorithm (MOCCA), which solves problems of the form (1) in the special case that $B = -\mathbf{I}$ and $c = 0$, i.e., our constraint is $Ax = y$. At a high level, the MOCCA algorithm can be viewed as a version of Algorithm 1 with a key modification: rather than taking a new linear approximation to f_d and g_d at each iteration (i.e., computing the gradients $\nabla f_d(x_t)$ and $\nabla g_d(y_t)$), the MOCCA algorithm requires an “inner loop”, where we cycle through the (x, u, y) update steps a finite number of times before re-calculating the linear approximations to f_d and g_d —in fact, in order to guarantee convergence, the number of iterations in each “inner loop” is required to grow. To our knowledge, this result is unique in that it ensures convergence without requiring either f or g to have a Lipschitz gradient (in comparison to the literature on ADMM in the nonconvex setting as discussed above), requiring instead a

restricted strong convexity type condition (see Section 3.2 below). However, the requirement of the “inner loop” to establish theoretical convergence contradicts the empirical performance of the algorithm, which typically shows convergence even if each “inner loop” is run for only a single update step—that is, there is no “inner loop” at all, in which case the algorithm becomes equivalent to the simpler and cleaner Algorithm 1.

2.2 Preview of new results

In the present work, we establish a convergence guarantee for Algorithm 1 in the nonconvex setting, with no “inner loop” needed in the theory, substantially closing the gap between the theoretical results and our empirical observations for this algorithm. As byproducts of this new analysis, we uncover an additional interesting finding that better explains the dependence of performance on step size parameters. Moreover, our new work allows for a more direct connection to CT imaging—we are able to apply our algorithm, exactly as defined and with no modifications, to simulated CT image reconstruction problems, obtaining very clean results. (For real CT data, issues of scanner calibration, non-random noise, etc. require a more careful application of the algorithm, which we address in separate work, but we mention here that the MOCCA algorithm has been very successful on real CT data, e.g., Schmidt et al. [2017, 2020].)

3 Convergence guarantee

We will prove a convergence result under an additional condition requiring approximate convexity of the problem. Before we can define our assumptions and state the result, we first need to examine the first-order optimality conditions of the problem.

3.1 First-order optimality

We observe that any first-order optimal solution to the minimization problem must consist of a triple (x, y, u) satisfying

$$\begin{cases} Ax + By = c, \\ -A^\top u \in \partial f(x), \\ -B^\top u \in \partial g(x). \end{cases} \quad (6)$$

Since f and g are not necessarily convex, we pause here to define our notation $\partial f(x)$ and $\partial g(y)$, which is a generalization of the usual subdifferential for convex functions. Here we will use the definition

$$\partial f(x) = \left\{ h : \lim_{t \rightarrow 0} \frac{f(x + tw) - f(x)}{t} \geq \langle h, w \rangle \text{ for all } w \in \text{dom}(f) - x \right\}$$

and similarly for g . In particular, given the convex+differentiable decomposition $f = f_c + f_d$, we can write

$$\partial f(x) = \{w + \nabla f_d(x) : w \in \partial f_c(x)\} \quad \text{and} \quad \partial g(y) = \{w : \nabla g_d(y) : w \in \partial g_c(y)\},$$

where $\partial f_c(x)$ and $\partial g_c(y)$ are the usual subdifferentials of the convex functions f_c and g_c , i.e.,

$$\partial f_c(x) = \{h : f(x+w) - f(x) \geq \langle h, w \rangle \text{ for all } w \in \text{dom}(f) - x\},$$

and similarly for g_c .

Our goal, then, is to establish conditions under which any first-order optimal point is (approximately) unique, and the nonconvex ADMM algorithm will converge to (approximately) this point.

3.2 Restricted strong convexity

We will assume a restricted strong convexity (RSC) condition, which at a high level is a relaxation of imposing a strong convexity condition on the constrained optimization problem. This type of convexity conditions has been extensively studied in the high-dimensional statistics literature. For background, the condition was proposed initially by Negahban et al. [2012], and was studied by Loh and Wainwright [2015] in the setting of nonconvex loss functions. This type of condition is known to characterize many settings where accurate signal recovery is possible in spite of the ‘‘curse of dimensionality’’, and over recent years has been studied in many settings, e.g., [Jain et al., 2014, Gunasekar et al., 2015, Elenberg et al., 2018].

To motivate this condition, first observe that if the function f were α -strongly convex then we would have $\langle x - \hat{x}, \partial f(x) - \partial f(\hat{x}) \rangle \geq \alpha \|x - \hat{x}\|_2^2$ (holding for any elements of the subdifferentials $\partial f(x)$ and $\partial f(\hat{x})$, if these are not singleton sets). Since $-A^\top \hat{u} \in \partial f(\hat{x})$ by definition, in particular we would have $\langle x - \hat{x}, \partial f(x) + A^\top \hat{u} \rangle \geq \alpha \|x - \hat{x}\|_2^2$. Similarly if g were α -strongly convex we would have $\langle y - \hat{y}, \partial g(y) + B^\top \hat{u} \rangle \geq \alpha \|y - \hat{y}\|_2^2$. If these functions are not individually strongly convex (or may even be nonconvex) but strong convexity is regained once we impose the constraint $Ax + By = c$, we might instead have a bound of the form

$$\left\langle \begin{pmatrix} x - \hat{x} \\ y - \hat{y} \end{pmatrix}, \begin{pmatrix} \partial f(x) + A^\top \hat{u} \\ \partial g(y) + B^\top \hat{u} \end{pmatrix} \right\rangle \geq \alpha (\|x - \hat{x}\|_2^2 + \|y - \hat{y}\|_2^2) \text{ for all } x, y \text{ s.t. } Ax + By = c,$$

which would of course be implied by strong convexity of f and of g , but is a strictly weaker condition.

In order to accommodate the setting of ADMM, where the constraint $Ax + By = c$ is not satisfied exactly at finite iterations, we will need to extend the statement above to allow for points that violate this constraint. We will assume the following condition:

Assumption 1 (Restricted Strong Convexity). *There exists a first-order optimal point $(\hat{x}, \hat{y}, \hat{u})$, constant $\varepsilon \geq 0$, matrix $\Sigma \succeq 0$, and convex nonnegative functions ψ_f, ψ_g such that the bound*

$$\left\langle \begin{pmatrix} x - \hat{x} \\ y - \hat{y} \end{pmatrix}, \begin{pmatrix} v_x - v_{\hat{x}} \\ w_y - w_{\hat{y}} \end{pmatrix} \right\rangle \geq \psi_f(x - \hat{x}) + \psi_g(y - \hat{y}) - \frac{1}{2} \|Ax + By - c\|_\Sigma^2 - \varepsilon^2, \quad (7)$$

for all $x \in \text{dom}(f)$, $y \in \text{dom}(g)$, and all $v_x \in \partial f(x)$, $v_{\hat{x}} \in \partial f(\hat{x})$, $w_y \in \partial g(y)$, $w_{\hat{y}} \in \partial g(\hat{y})$.

In particular, when running nonconvex ADMM with a penalty matrix Σ , we will require this condition to hold with this same matrix Σ .

In many common settings we may choose to take $\psi_f(\cdot) = \alpha\|\cdot\|_2^2$ and/or $\psi_g(\cdot) = \alpha\|\cdot\|_2^2$ for some positive constant α , meaning that the RSC property offers strong convexity in feasible directions (i.e., (x, y) such that $Ax + By = c$). On the other hand, the parameter ε is typically vanishing. For example, if the optimization problem arises from a statistical question where we would like to estimate parameters based on a sample of size n , we would aim to establish an RSC condition with the slack variable ε on the order of $n^{-1/2}$ (convergence beyond this accuracy level is not informative, since a sample of size n can only recover parameters up to errors of order $n^{-1/2}$ even with limitless computational resources).

3.2.1 Comparing RSC to the augmented Lagrangian

To better understand this condition in the setting of the composite optimization problem (1) studied in this work, consider the augmented Lagrangian \mathcal{L}_Σ defined in (3). Since the x and y update steps of ADMM are performing (approximate) alternating minimization on this augmented Lagrangian, it is intuitive that convexity of the map $(x, y) \mapsto \mathcal{L}_\Sigma(x, y, u)$ (at a fixed u) is generally needed for convergence to be possible.

On the other hand, if $(x, y) \mapsto \mathcal{L}_{\Sigma/2}(x, y, u)$ is strongly convex (note that we have replaced the penalty matrix Σ with a smaller penalty, $\Sigma/2$), this is sufficient to ensure the restricted strong convexity condition (7), since an elementary calculation shows that

$$\begin{aligned} \left\langle \begin{pmatrix} x - \hat{x} \\ y - \hat{y} \end{pmatrix}, \begin{pmatrix} \partial f(x) - \partial f(\hat{x}) \\ \partial g(y) - \partial g(\hat{y}) \end{pmatrix} \right\rangle + \frac{1}{2} \|Ax + By - c\|_\Sigma^2 \\ = \left\langle \begin{pmatrix} x - \hat{x} \\ y - \hat{y} \end{pmatrix}, \nabla_{(x,y)} \mathcal{L}_{\Sigma/2}(x, y, u) - \nabla_{(x,y)} \mathcal{L}_{\Sigma/2}(\hat{x}, \hat{y}, u) \right\rangle \end{aligned}$$

using the fact that $A\hat{x} + B\hat{y} = c$ by feasibility; the right-hand side will be lower-bounded by strong convexity of $\mathcal{L}_{\Sigma/2}$. Therefore, we can interpret the RSC condition (7) as only mildly stronger than requiring strong convexity of the augmented Lagrangian.

The RSC property also provides some insight into the role of the ADMM step size parameter (the matrix Σ in our notation, but typically denoted by a scalar ρ in the ADMM literature). We can see that, in the presence of nonconvexity—or even if the problem is convex, but not globally strongly convex—the RSC property may fail if Σ is chosen to be too small. In our empirical results in Section 4, we will see in a concrete example that empirically we may observe failure to converge for smaller Σ while larger Σ enables stable convergence.

3.2.2 RSC implies uniqueness

Before proving our convergence result, we first pause to verify that the RSC condition (7) is sufficient to ensure uniqueness, or approximately uniqueness, of the first-order stationary point $(\hat{x}, \hat{y}, \hat{u})$. (In fact, without such a result, any convergence statement would be poorly defined since we would not have a way of uniquely specifying the target that we wish to converge to.)

Lemma 1. *Suppose that there exists some first-order optimal point $(\hat{x}, \hat{y}, \hat{u})$, such that*

$$\begin{aligned} & \left\langle \begin{pmatrix} x - \hat{x} \\ y - \hat{y} \end{pmatrix}, \begin{pmatrix} \partial f(x) + A^\top \hat{u} \\ \partial g(y) + B^\top \hat{u} \end{pmatrix} \right\rangle \\ & \geq \psi_f(x - \hat{x}) + \psi_g(y - \hat{y}) - \varepsilon^2 \text{ for all } (x, y, u) \text{ with } Ax + By = c. \end{aligned}$$

Then for any point (x, y, u) satisfying the first-order optimality conditions (6), it holds that

$$\psi_f(x - \hat{x}) + \psi_g(y - \hat{y}) \leq \varepsilon^2.$$

In particular, if the RSC assumption (7) holds with any $\Sigma \succeq 0$, then the conditions of this lemma will hold. In settings where $\psi_f(x - \hat{x})$ and $\psi_g(y - \hat{y})$ bound the error magnitudes $\|x - \hat{x}\|_2$ and $\|y - \hat{y}\|_2$, this then yields a guarantee that (x, y) must be close to (\hat{x}, \hat{y}) .

Proof of Lemma 1. Let (x, y, u) be any point satisfying (6). Then by the assumption in the lemma, together with conditions (6) on the points (x, y, u) and $(\hat{x}, \hat{y}, \hat{u})$, we have

$$\begin{aligned} & \psi_f(x - \hat{x}) + \psi_g(y - \hat{y}) - \varepsilon^2 \\ & \leq \left\langle \begin{pmatrix} x - \hat{x} \\ y - \hat{y} \end{pmatrix}, \begin{pmatrix} \partial f(x) + A^\top \hat{u} \\ \partial g(y) + B^\top \hat{u} \end{pmatrix} \right\rangle = \left\langle \begin{pmatrix} x - \hat{x} \\ y - \hat{y} \end{pmatrix}, \begin{pmatrix} -A^\top u + A^\top \hat{u} \\ -B^\top u + B^\top \hat{u} \end{pmatrix} \right\rangle \\ & \quad = -\langle u - \hat{u}, Ax + By - A\hat{x} - B\hat{y} \rangle = -\langle u - \hat{u}, c - c \rangle = 0. \end{aligned}$$

□

3.3 Main result: convergence guarantee

Our main result proves that the ADMM iterates (x_t, y_t, u_t) converge to $(\hat{x}, \hat{y}, \hat{u})$ (up to the error level ϵ), as long as we choose the step size matrices H_f, H_g to satisfy

$$\begin{cases} H_f \succeq 0, \text{ and } H_f \succeq \nabla^2 f_d(x) \text{ for all } x \in \text{dom}(f), \\ H_g \succeq 0, \text{ and } H_g \succeq \nabla^2 g_d(y) \text{ for all } y \in \text{dom}(g). \end{cases} \quad (8)$$

We note that, if f_d (respectively g_d) is concave, then the corresponding step size matrix H_f (respectively H_g), can be chosen to be zero. However, even in this case, we may prefer to take a nonzero step size matrix for easier update step calculations, as discussed above.

Theorem 1. *Assume that the restricted strong convexity condition (7) holds relative to some first-order optimal point $(\hat{x}, \hat{y}, \hat{u})$, for some $\Sigma \succeq 0$. Suppose that the nonconvex ADMM algorithm given in Algorithm 1 is run with this choice of the penalty matrix Σ and with step size matrices H_f, H_g satisfying (8), initialized at an arbitrary point (x_0, y_0, u_0) where $x_0 \in \text{dom}(f)$ and $y_0 \in \text{dom}(g)$.*

Define

$$\bar{x}_T = \frac{1}{T} \sum_{t=1}^T x_t \text{ and } \bar{y}_T = \frac{1}{T} \sum_{t=1}^T y_t,$$

where x_t, y_t are the iterates of the nonconvex ADMM algorithm. Then for all $T \geq 1$, it holds that

$$\psi_f(\bar{x}_T - \hat{x}) + \psi_g(\bar{y}_T - \hat{y}) \leq \frac{C(\hat{x}, \hat{y}, \hat{u}; x_0, y_0, u_0)}{T} + \varepsilon^2,$$

where the function C is defined explicitly in the proof, and does not depend on the iteration number T .

In particular, if f_d and g_d have Lipschitz gradients, we will see that $C(x, y, u; x_0, y_0, u_0) = \mathcal{O}(\|(x, y, u) - (x_0, y_0, u_0)\|_2^2)$, so that

$$\psi_f(\bar{x}_T - \hat{x}) + \psi_g(\bar{y}_T - \hat{y}) \leq \frac{\mathcal{O}(\|(x, y, u) - (x_0, y_0, u_0)\|_2^2)}{T} + \varepsilon^2.$$

Comparison to related work In Section 2.1.2, we discussed prior work on different variants of the nonconvex ADMM algorithm (with or without linear approximations to the differentiable components f_d and g_d of the objective function). These existing results all require that at least one of the two functions (f or g) must be smooth, or alternatively proves a weaker convergence result, establishing properties of the limit point under the assumption that the algorithm converges (without proving that convergence must occur). The related MOCCA algorithm, discussed in Section 2.1.3, does allow for both f and g to be nonsmooth, but the convergence guarantee comes at the cost of an “inner loop” in the algorithm that increases in length with every iteration, which would be extremely inefficient in practice. The contribution of Theorem 1 is that we can be assured that the nonconvex ADMM algorithm will converge even when both f and g are nonsmooth, by leveraging the more flexible RSC property.

3.4 Proof of Theorem 1

Fix any point (x, y, u) satisfying $Ax + By = c$. In Appendix A.1, we will prove that the assumption (8) on the step size matrices H_f, H_g ensures that, for all $T \geq 1$,

$$\begin{aligned} \sum_{t=0}^{T-1} \left\langle \begin{pmatrix} x_{t+1} - x \\ y_{t+1} - y \end{pmatrix}, \begin{pmatrix} \partial f(x_{t+1}) + A^\top u \\ \partial g(y_{t+1}) + B^\top u \end{pmatrix} \right\rangle + \frac{1}{2} \sum_{t=0}^{T-1} \|Ax_{t+1} + By_{t+1} - c\|_\Sigma^2 \\ \leq C(x, y, u; x_0, y_0, u_0), \end{aligned} \quad (9)$$

where this bound is only required to hold for *some* choice of subgradients $\partial f(x_{t+1})$ and $\partial g(y_{t+1})$, for each t (i.e., if these subgradients are not unique in the case of nondifferentiable functions). The function C will be defined in the Appendix (see (20)).

Assuming for now that this bound holds, we will apply it at the point $(x, y, u) = (\hat{x}, \hat{y}, \hat{u})$. Applying the restricted strong convexity assumption (7), this means that

$$\begin{aligned} \left\langle \begin{pmatrix} x_{t+1} - \hat{x} \\ y_{t+1} - \hat{y} \end{pmatrix}, \begin{pmatrix} \partial f(x_{t+1}) + A^\top \hat{u} \\ \partial g(y_{t+1}) + B^\top \hat{u} \end{pmatrix} \right\rangle \\ \geq \psi_f(x_{t+1} - \hat{x}) + \psi_g(y_{t+1} - \hat{y}) - \frac{1}{2} \|Ax_{t+1} + By_{t+1} - c\|_\Sigma^2 - \varepsilon^2. \end{aligned}$$

Combined with (9) above, and rearranging terms, we obtain

$$\sum_{t=0}^{T-1} (\psi_f(x_{t+1} - \hat{x}) + \psi_g(y_{t+1} - \hat{y})) \leq C(\hat{x}, \hat{y}, \hat{u}; x_0, y_0, u_0) + T\varepsilon^2.$$

In particular, by convexity of ψ_f and ψ_g this implies that

$$\psi_f(\bar{x}_T - \hat{x}) + \psi_g(\bar{y}_T - \hat{y}) \leq \frac{C(\hat{x}, \hat{y}, \hat{u}; x_0, y_0, u_0)}{T} + \varepsilon^2,$$

which completes the proof.

4 Example: sparse high-dimensional quantile regression

In this section, we will develop a concrete example of our framework, to illustrate the empirical performance and convergence properties of our method. Consider a regression setting where

$$w_i = \phi_i^\top x_* + (\text{noise}), \quad i = 1, \dots, n,$$

for a sparse true signal $x_* \in \mathbb{R}^d$. The response variables $w_i \in \mathbb{R}$ and the sensing matrix $\Phi = (\phi_1, \dots, \phi_n)^\top \in \mathbb{R}^{n \times d}$ are observed, and our goal is to recover x_* . If the noise is heavy-tailed, then a standard least-squares regression may perform poorly, and we may prefer the more robust properties of a quantile regression. Specifically, for any desired quantile $q \in (0, 1)$, consider the quantile loss

$$\ell_q(t) = q \cdot \max\{t, 0\} + (1 - q) \cdot \max\{-t, 0\}.$$

Then if we seek to minimize

$$\sum_{i=1}^n \ell_q(w_i - \phi_i^\top x)$$

over $x \in \mathbb{R}^d$, this loss corresponds to aiming for $\phi_i^\top x$ to equal the q -th quantile of w_i .

In the high-dimensional setting where $n < d$, minimizing this loss is not meaningful (in general, we can find a vector $x \in \mathbb{R}^d$ that interpolates the data, i.e., $\phi_i^\top x = w_i$ for all i , which clearly leads to overfitting). We will therefore consider a penalized version of this loss:

$$\arg \min_{x \in \mathbb{R}^d} \left\{ \sum_{i=1}^n \ell_q(w_i - \phi_i^\top x) + \lambda \sum_{j=1}^d \beta \log(1 + |x_j|/\beta) \right\}. \quad (10)$$

The last term is a nonconvex regularizer that encourages a sparse solution. For $\beta = +\infty$, the regularizer is equal to the ℓ_1 norm, a standard convex penalty for recovering sparse signals, while $\beta < +\infty$ leads to a nonconvex penalty. Smaller values of β correspond to greater nonconvexity, which makes the optimization problem more challenging but comes with the benefit of less shrinkage on the nonzero values in the signal vector x (see Figure 4).

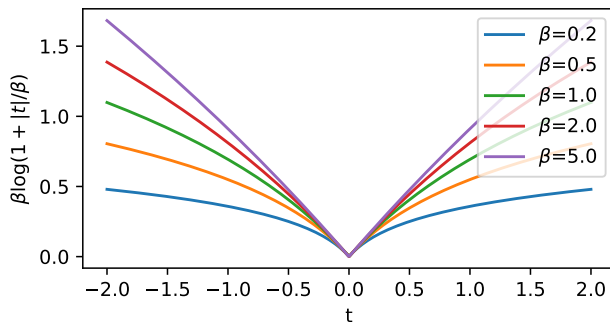


Figure 1: Illustration of the nonconvex sparsity-promoting penalty $\sum_j \beta \log(1 + |x_j|/\beta)$ that appears in the objective function (10) for the sparse high-dimensional quantile regression example. The figure plots the function $t \mapsto \beta \log(1 + |t|/\beta)$, for each $\beta \in \{1, 2, 10, \infty\}$. (At the limit point $\beta = \infty$, the function is equal to the absolute value function, $t \mapsto |t|$.) The functions are all nondifferentiable at $t = 0$, and are similar to the absolute value function for $t \approx 0$, but smaller values of β correspond to greater nonconvexity as $|t|$ increases.

4.1 Implementing nonconvex ADMM

For the sparse quantile regression problem (10), we will introduce an additional variable y (with the constraint $y = \Phi x$) so that the optimization problem can be solved with Algorithm 1—we will minimize

$$\arg \min_{x \in \mathbb{R}^d, y \in \mathbb{R}^n} \left\{ \sum_{i=1}^n \ell_q(w_i - y_i) + \lambda \sum_{j=1}^d \beta \log(1 + |x_j|/\beta) : y = \Phi x \right\}.$$

To solve (10), we will run Algorithm 1 with parameters $\Sigma = \sigma \mathbf{I}_n$, $H_f = \sigma(\gamma \mathbf{I}_d - \Phi^\top \Phi)$ (with $\gamma = \|\Phi\|^2$ so that $H_f \succeq 0$), and $H_g = 0$, and with functions

$$f_c(x) = \lambda \sum_{j=1}^d |x_j|, \quad f_d(x) = \lambda \sum_{j=1}^d (\beta \log(1 + |x_j|/\beta) - |x_j|)$$

and

$$g_c(y) = \sum_{i=1}^n \ell_q(w_i - y_i), \quad g_d(y) \equiv 0.$$

The update steps for Algorithm 1 can be calculated in closed form (details are given in Appendix A.2). We note that the function f_d is concave and twice differentiable, with $\nabla^2 f_d(x) \succeq -\lambda \beta^{-1} \mathbf{I}_d$ for all x , so its concavity is bounded.

4.2 Empirical results

We next demonstrate the performance of our algorithm on the sparse quantile regression problem. Code reproducing the simulation and all figures is available on the authors' website.¹

¹https://www.stat.uchicago.edu/~rina/nonconvex_admm_ct.html

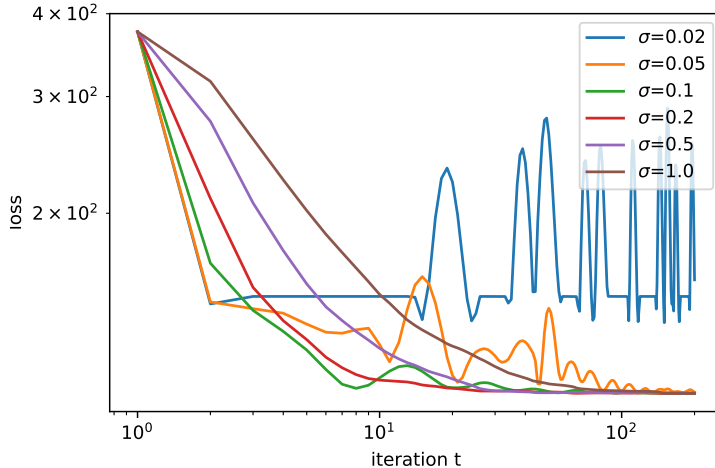


Figure 2: Results for the sparse quantile regression example (see Section 4.2). The figure shows the value of the objective function (10) over iteration $t = 1, \dots, 200$ of the algorithm, run with various values of the parameter σ as shown. Both axes are on the log scale.

We choose dimension $d = 500$ and sample size $n = 200$ for a challenging high-dimensional setting. The matrix $\Phi \in \mathbb{R}^{n \times d}$ is constructed with i.i.d. $\mathcal{N}(0, \frac{1}{n})$ entries. We define

$$w_i = \phi_i^\top x_* + \varepsilon_i,$$

where ϕ_i is the i th row of Φ , and the true signal is given by $x_* = (10, 10, 10, 10, 10, 0, \dots, 0)$. The noise terms ε_i are drawn i.i.d. from t_5 , the standard t distribution with 5 degrees of freedom, which is a heavy-tailed distribution. We choose the quantile $q = 0.5$ (i.e., a median regression). For the penalty term, we choose $\lambda = 1$ and $\beta = 0.5$, ensuring substantial nonconvexity in the penalty. The parameter σ controlling the enforcement of the constraint in ADMM (i.e., with $\Sigma = \sigma \mathbf{I}_d$ in Algorithm 1) is varied as $\sigma \in \{0.02, 0.05, 0.1, 0.2, 0.5, 1.0\}$.

The results after running Algorithm 1 for 200 iterations are displayed in Figure 2. The plot displays the loss at each iteration t , i.e., the value of the objective function (10) evaluated at the current estimate x_t . We see that overly small values of σ lead to unstable behavior or even failure to converge, which is supported qualitatively by our theory—in particular, we need $\Sigma = \sigma \mathbf{I}_d$ to be sufficiently large in order for the composite RSC condition (7) to hold. On the other hand, overly large values of σ may lead to somewhat slower convergence (intuitively, enforcing the constraint $y = \Phi x$ with too strong of a penalty will make it difficult for the algorithm to make fast progress with alternating updates of x and y).

Comparing to theoretical setting Our theoretical results guarantee convergence for the nonconvex ADMM algorithm as long as the RSC property (7) holds. In fact, there exist results in the literature establishing a RSC-type property for sparse high-dimensional quantile regression, e.g., see Sivakumar and Banerjee [2017, Theorem 4.2, Corollary 7] and Belloni and Chernozhukov [2011, Lemma 4]; the conditions proved in the literature appear in a different

form than the RSC property studied here, but are similar in flavor. (Resolving the differences between the forms of the property is possible with some mild additional conditions, but is highly technical and so we do not address this here.) In contrast, as discussed in Section 2.1.2, existing results establishing convergence for nonconvex ADMM assume, at minimum, that either f or g is differentiable and has a Lipschitz gradient. We can see immediately that this property is violated for the sparse quantile regression problem (10), since the functions f and g are both nondifferentiable. Therefore, this example illustrates the flexibility and broad applicability of RSC type assumptions, as compared to other assumptions in the literature.

5 Application: CT imaging

We next apply our algorithm and convergence results to the problem of image reconstruction in computed tomography (CT) imaging, which is the motivating application for this work. In CT, we would like to reconstruct an image of an unknown object x (e.g., produce a 3D image of a patient’s abdomen, in the setting of medical CT). The available measurements obtained from the CT scanner consist of measuring the intensity of an X-ray beam passing through the unknown object. A lower intensity of the beam when it reaches the detector indicates higher density in the unknown object along that ray.

We now introduce some notation to make this problem more precise. We will begin with a simple version of the problem, and then will add additional components step by step to build intuition. Let $x = (x_k) \in \mathbb{R}^{n_k}$ denote the unknown image, where $k = 1, \dots, n_k$ indexes pixels (or voxels), after we have discretized to a 2D (or 3D) grid (for example, in two dimensions, $n_k = N_x \cdot N_y$ for an $N_x \times N_y$ grid).

To obtain an image, the scanner sends an X-ray beam along n_ℓ many rays. For example, for many clinical scanners in a medical setting, the device rotates around the patient, taking images from N_{img} many angles; for each of these images, there are N_{cell} many detector cells measuring the intensity of the beam after it passes through the patient’s body. This leads to $n_\ell = N_{\text{img}} \cdot N_{\text{cell}}$ many rays $\ell = 1, \dots, n_\ell$ along which measurements are taken.

Now let $P = (P_{\ell k}) \in \mathbb{R}^{n_\ell \times n_k}$ be the projection matrix, with $P_{\ell k}$ measuring the length of the intersection between ray ℓ and pixel k . The product $Px \in \mathbb{R}^{n_\ell}$ measures the projection of the object x , where $(Px)_\ell$ measures the total amount of material that lies along ray ℓ (see Figure 3 for a schematic). The attenuation (i.e., the loss of intensity) of the X-ray beam that travels along ray ℓ depends on $(Px)_\ell$. In particular, ignoring photon scattering and other sources of noise, the measurements follow a model of the form

$$\frac{\text{Intensity of the beam after passing through the object along ray } \ell}{\text{Intensity of the beam entering the object along ray } \ell} \approx e^{-\mu \cdot (Px)_\ell},$$

where $\mu > 0$ is called the linear attenuation coefficient. While most clinical scanners measure the total energy of the beam when it reaches the detector, here we consider a different type of hardware, *photon counting CT*, where the measurement is a count of the number of photons reaching the detector. In this case, we can model this count as

$$C_\ell \sim \text{Poisson}(S \cdot \exp\{-\mu \cdot (Px)_\ell\}),$$

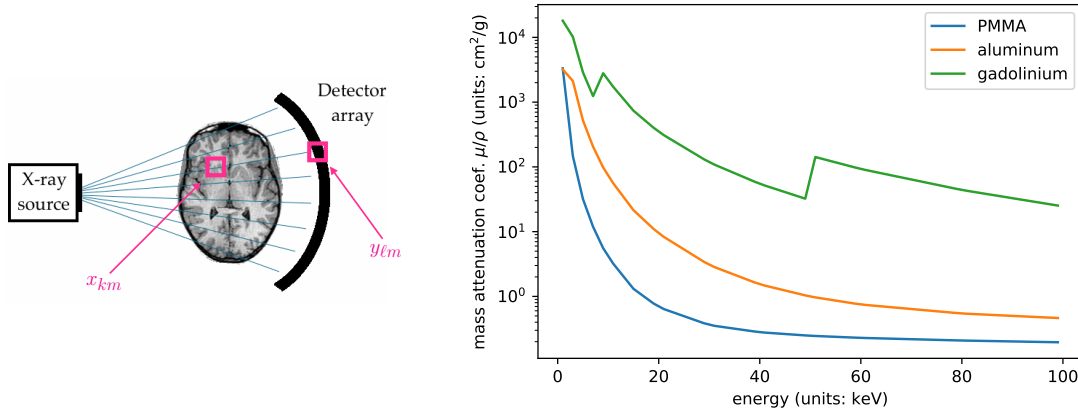


Figure 3: Left: schematic of the projection operator. Here x_{km} is the amount of material m present at pixel k , while $y_{\ell m} = (Px)_{\ell m}$ is the total amount of material m present along ray ℓ of the scan. Right: attenuation curves for several common materials.

where S is the number of photons incident on the detector pixel (characterizing the intensity of the X-ray beam for a fixed time-duration scan), and C_ℓ is the number of photons reaching detector after passing through the object along ray ℓ .

In fact, since different detector cells may have slightly different sensitivities, a more accurate model is

$$C_\ell \sim \text{Poisson}(S_\ell \cdot \exp\{-\mu \cdot (Px)_\ell\}), \quad (11)$$

where the scalar term S_ℓ combines beam intensity with detector sensitivity.

Multiple materials In practice, the unknown object can consist of multiple materials, which each behave differently in terms of the attenuation of the beam. Let $m = 1, \dots, n_m$ index the materials that make up the object—for example, in a simple medical setting we might have $n_m = 3$ with bone, soft tissue, and an injected contrast material such as iodine. The goal is now to reconstruct the image $x = (x_{km}) \in \mathbb{R}^{n_k \times n_m}$, where x_{km} measures the density of material m present in pixel k . We can update our model (11) above to

$$C_\ell \sim \text{Poisson}\left(S_\ell \cdot \exp\left\{-\sum_m \mu_m \cdot (Px)_{\ell m}\right\}\right), \quad (12)$$

where now $\mu_m > 0$ is the attenuation coefficient for material m .

A non-monochromatic beam Thus far, the Poisson model for CT image reconstruction does not introduce nonconvexity—maximizing the log-likelihood of the Poisson model given in (12) is a convex problem. However, this model ignores the nature of the X-ray beam used in practice, for which the photons are distributed across a spectrum of energies. The attenuation coefficient for a material m in fact depends on the energy of the photon, with each material exhibiting its own attenuation curve across the range of energies—see Figure 3

for an example. In particular, in medical applications, contrast materials such as gadolinium or iodine are used for their unique attenuation curves, which make these materials easier to distinguish from surrounding soft tissue in a CT scan.

Our model can now be updated to the following:

$$C_\ell \sim \text{Poisson} \left(\sum_i S_{\ell i} \cdot \exp \left\{ - \sum_m \mu_{mi} (Px)_{\ell m} \right\} \right), \quad (13)$$

where $i = 1, \dots, n_i$ is the index over a discretized grid of the range of energies in the X-ray beam, while $S_{\ell i}$ is the intensity of the X-ray beam (combined with detector sensitivity) for energy level i , and μ_{mi} is the attenuation coefficient for material m at energy level i . The photons measured by the detector may come from any energy level in the spectrum (i.e., the measurements C_ℓ are a combination of photons from each energy level i). The resulting log-likelihood maximization problem is no longer a convex function, which is a core challenge of CT image reconstruction.

Spectral CT In spectral CT, the hardware of the scanner allows partial identification of the photon energies, making the reconstruction problem somewhat easier. Specifically, the detectors are programmed with several thresholds, separating the range of energies of the beam into “windows” $w = 1, \dots, n_w$ (for example, 2 windows in some current clinical scanners, or 3–5 windows in current research prototypes). The measurements are now indexed by $C_{w\ell}$, the number of photons in energy window w measured along ray ℓ . In theory, the windows form a partition of the energy range, but in practice there is some noise at the boundaries between windows (that is, a photon with energy near the chosen threshold has some chance of being detected in either window). To quantify this, let S_{wli} incident photon spectral density at energy i , multiplied by the probability of a photon at energy i being detected in window w (for the detector sensitivity corresponding to ray ℓ). These values are typically estimated ahead of time with a calibration process. Then the model for our measurements $C_{w\ell}$ is given by

$$C_{w\ell} \sim \text{Poisson} \left(\sum_i S_{wli} \cdot \exp \left\{ - \sum_m \mu_{mi} (Px)_{\ell m} \right\} \right). \quad (14)$$

We can estimate the image x by maximum likelihood estimation, but as before in (13), maximizing the log-likelihood is a non-convex problem.

5.1 Image reconstruction with nonconvex ADMM

We now consider the image reconstruction problem: given observations (photon counts) $C_{w\ell}$, we would like to solve

$$\hat{x} = \underset{x \in \mathbb{R}^{n_k \times n_m}}{\text{arg min}} \text{Loss}(Px), \quad (15)$$

where $\text{Loss}(y)$ is the negative log-likelihood of the Poisson model for spectral CT (14) given the projected object $y = Px \in \mathbb{R}^{n_\ell \times n_m}$:

$$\text{Loss}(y) = \sum_{w\ell} \left[\sum_i S_{wli} \exp \left\{ - \sum_m \mu_{mi} y_{\ell m} \right\} - C_{w\ell} \log \left(\sum_i S_{wli} \exp \left\{ - \sum_m \mu_{mi} y_{\ell m} \right\} \right) \right].$$

We note that the first term of this loss is convex in y (and therefore, in x), while the second term is concave.

Modifying the exp function Under a well-specified model, the true image x and its projection $y = Px$ must both consist of nonnegative values. However, model misspecification, or inaccurate estimates of x and/or y at early stages of the iterative algorithm, can lead to negative values. Examining the loss function, we can see that this issue may pose problems for optimization, since $t \mapsto \exp\{t\}$ has high curvature at large values of t . To resolve this, we replace the $\exp\{\cdot\}$ function with the approximation:

$$\text{qexp}\{t\} = \begin{cases} \exp\{t\}, & t \leq 0, \\ 1 + t + \frac{1}{2}t^2, & t \geq 0. \end{cases}$$

The “q” in the name of this modified function refers to the fact that, for positive values of t we replace $\exp\{t\}$ with a quadratic approximation, by taking the Taylor expansion at $t = 0$. For negative values of t , the function is unchanged. This choice means that the function $\text{qexp}\{t\}$ is continuously twice differentiable and is equal to $\exp\{t\}$ at all negative values of t (i.e., for any feasible nonnegative image x), while at the same time ensuring a bounded second derivative to avoid problems in the optimization. We will therefore work with a modified loss function,

$$\text{Loss}(y) = \sum_{w\ell} \left[\sum_i S_{w\ell i} \text{qexp} \left\{ - \sum_m \mu_{mi} y_{\ell m} \right\} - C_{w\ell} \log \left(\sum_i S_{w\ell i} \text{qexp} \left\{ - \sum_m \mu_{mi} y_{\ell m} \right\} \right) \right].$$

It is important to note that, for CT imaging, if the model is well specified then the true value of y should be nonnegative, since $y = Px$ where the projection matrix P is nonnegative by definition, and the entries of x represent material densities and should therefore be nonnegative as well. Therefore, $\text{qexp}\{\cdot\}$ should be identical to $\exp\{\cdot\}$ in the relevant range of values. (Empirically, the convergence behavior of the optimization problem is often helped by allowing negative values, particularly in early iterations.)

Running nonconvex ADMM To reformulate the minimization problem (15) into the setting of nonconvex ADMM, we will create a new variable $y \in \mathbb{R}^{n_\ell \times n_m}$, and will solve the equivalent problem

$$\hat{x}, \hat{y} = \arg \min_{\substack{x \in \mathbb{R}^{n_k \times n_m} \\ y \in \mathbb{R}^{n_\ell \times n_m}}} \{\text{Loss}(y) : Px = y\}. \quad (16)$$

Now define $f(x) = f_c(x) = f_d(x) \equiv 0$, and write $g(y) = g_c(y) + g_d(y)$ where

$$g_c(y) = \sum_{w\ell} \sum_i S_{w\ell i} \text{qexp} \left\{ - \sum_m \mu_{mi} y_{\ell m} \right\} \quad (17)$$

and

$$g_d(y) = - \sum_{w\ell} C_{w\ell} \log \left(\sum_i S_{w\ell i} \text{qexp} \left\{ - \sum_m \mu_{mi} y_{\ell m} \right\} \right).$$

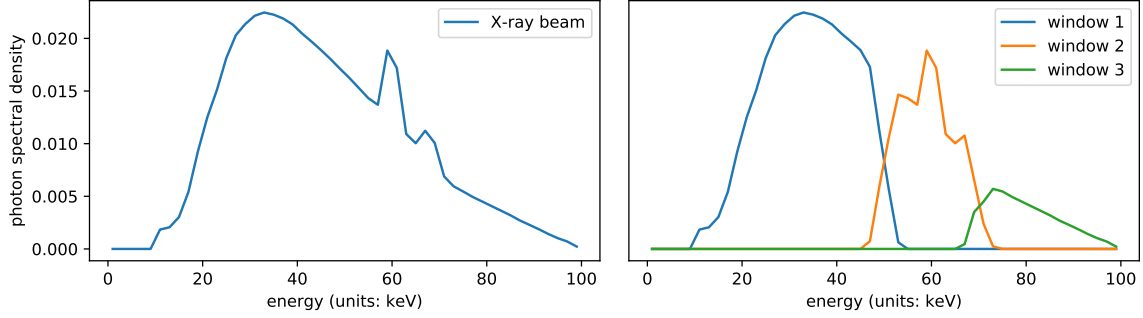


Figure 4: Left: the X-ray beam spectrum. This figure displays the density of the distribution of energies in the beam, i.e., how the total intensity of the beam is split across the energy spectrum. Right: for each energy window w , the displayed curve is proportional to the spectral response parameters $S_{w\ell i}$. These values are set to be constant across all rays ℓ , and so the figure plots the value across all energy levels i for each detector window w , rescaled so that the sum of the three response curves is equal to the density plot of the X-ray beam spectrum on the left.

Then $\text{Loss}(y) = g(y)$, and we have therefore reformulated the spectral CT maximum likelihood estimation problem into the form of our nonconvex ADMM algorithm, i.e., $\min_{x,y} \{f(x) + g(y) : Ax + By = c\}$, with $A = P$, $B = -\mathbf{I}$, and $c = 0$. We can therefore implement Algorithm 1 for solving this optimization problem. To run Algorithm 1 for the CT image reconstruction problem 16, we need to choose the step size matrices H_f, H_g and the penalty matrix Σ . Following the construction proposed by Pock and Chambolle [2011] (for the convex setting), we begin by selecting a parameter $\sigma > 0$). We will choose step size matrix $H_g = 0$ for y , while for the variable x our step size matrix H_f will be equal to $H_f = Q_f - P^\top \Sigma P$ where Q_f and Σ are diagonal matrices with entries

$$(Q_f)_{km,km} = \sigma \sum_{\ell} P_{\ell k}, \quad \Sigma_{\ell m, \ell m} = \frac{\sigma}{\sum_k P_{\ell k}}.$$

These constructions ensure that H_f is positive semidefinite, as required. The update steps are shown in Appendix A.3.

5.2 CT simulation

To demonstrate the algorithm’s performance on the nonconvex CT image reconstruction problem, we carry out a small-scale simulation in Python. (Performance of these methods on a large scale requires more careful implementation, and is addressed in our application specific work in Barber et al. [2016], Schmidt et al. [2020].) Code reproducing the simulation and all figures is available on the authors’ website.²

The ground truth, shown in Figure 5, is a $10\text{cm} \times 10\text{cm}$ two-dimensional image discretized to a 25×25 grid, for a total of $n_k = 25^2 = 625$ pixels. The image consists of $n_m = 3$

²https://www.stat.uchicago.edu/~rina/nonconvex_admm_ct.html

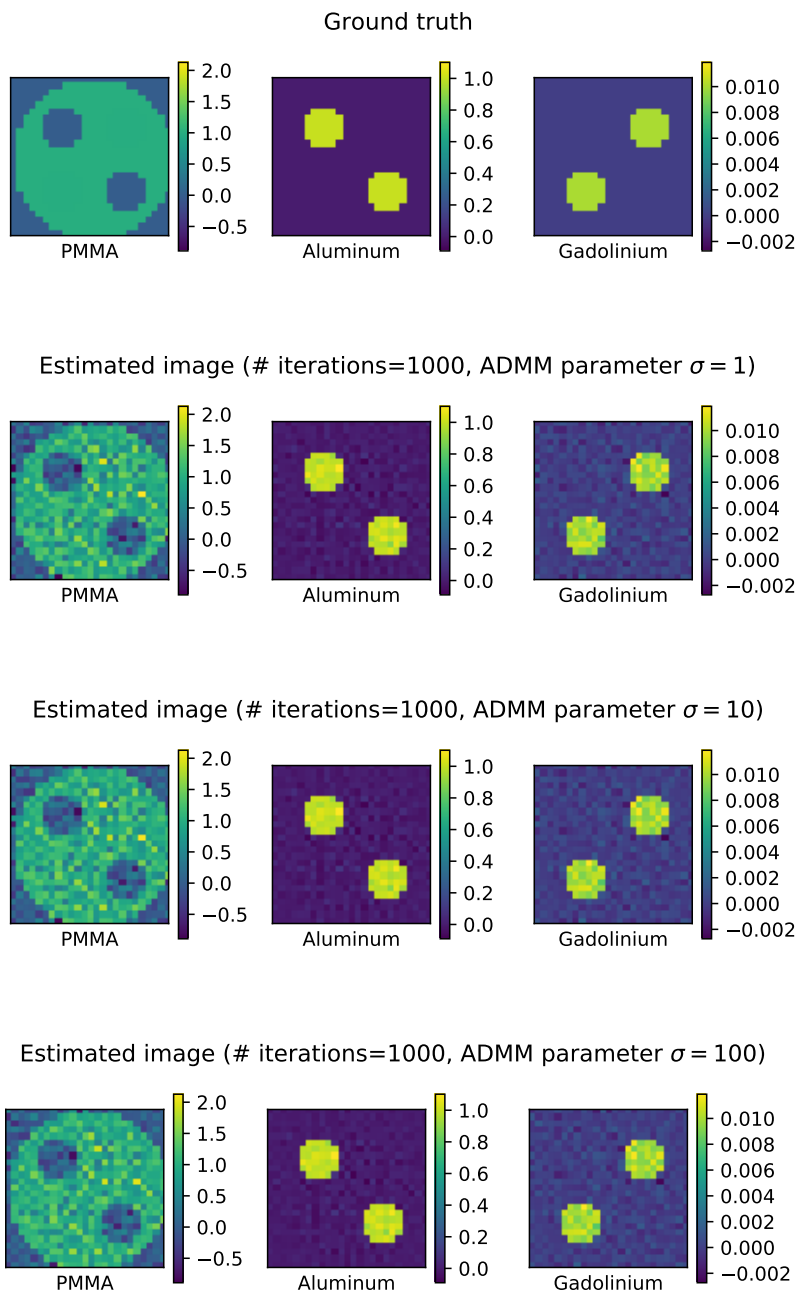


Figure 5: The true image in the simulation (top), followed by the reconstructed image (at iteration 1000) with each value of the ADMM parameter σ . For each pixel, the units are the (true or estimated) proportion of that pixel that is occupied by each material.

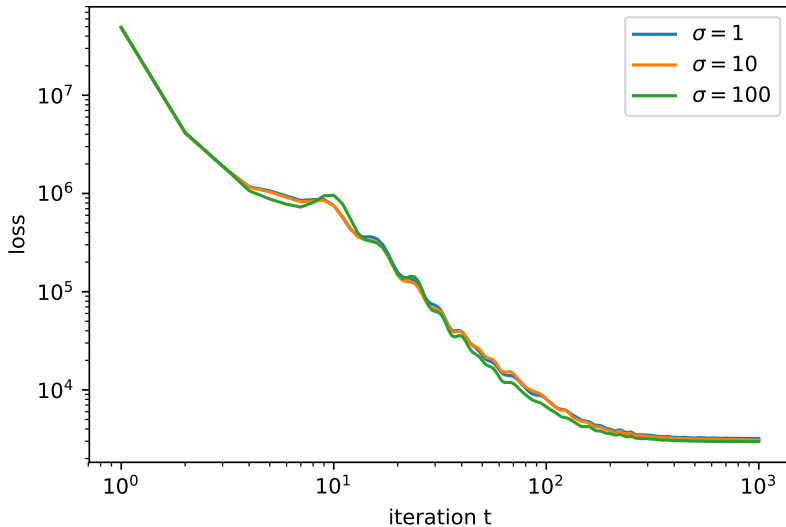


Figure 6: Convergence results for the CT image reconstruction simulation. The figure shows the value of the objective function $\text{Loss}(Px_t)$ over iteration $t = 1, \dots, 1000$ of the algorithm, run with various values of the parameter σ as shown. Both axes are on the log scale.

materials—polymethyl methacrylate (PMMA), aluminum, and gadolinium. As shown in Figure 3, PMMA has low attenuation coefficients as it is a plastic, while aluminum, like other metals, has higher attenuation coefficients as it is more difficult for the beam to pass through. Gadolinium is a contrast material used in clinical CT—its non-monotone attenuation curve allows for it to be easily identified in the presence of other materials. The simulated CT scanner has 50 detector cells, and takes images from 50 angles spaced evenly around the unit circle, for a total of $n_\ell = 50^2 = 2500$ rays along which measurements are taken. The beam intensity is set to 10^5 photons, and there are $n_w = 3$ energy windows, forming a blurry partition of the energy range (see Figure 4).

Figure 5 displays the estimated image (shown at iteration 1000, at each value of the ADMM parameter $\sigma \in \{1, 10, 100\}$). In Figure 6 we show the loss function $\text{Loss}(Px_t)$ at each iteration $t = 1, \dots, 1000$. The performance is quite similar across a wide range of σ values, showing that the algorithm is not overly sensitive to this tuning parameter in this particular example. The dependence of performance on σ may be different for other optimization problems, and in general this parameter should be tuned in order to optimize convergence rate. In Figure 6 we can see that the algorithm converges steadily towards minimizing the loss, although convergence is not very fast (as is often the case when ADMM is applied to poorly conditioned problems).

The objective function, and accompanying algorithm, that we have presented here, can easily be modified to incorporate additional components such as regularization or constraints. In particular, total variation regularization can also be incorporated into the framework of Algorithm 1 (details and a demonstration can be found on the authors’ website alongside the basic non-regularized simulation setting presented here). Another possible modification is adding a preconditioning step to improve the conditioning in the n_m -dimensional material space,

since the attenuation curves for the three materials are quite similar (see Figure 3), adding a preconditioning step can improve convergence substantially for the image reconstruction problem (see Sidky et al. [2018] for more details).

6 Discussion

The ADMM algorithm has long been known to perform well in a broad range of challenging scenarios, but existing theoretical analyses are largely restricted to a much more constrained range of settings. Our new theoretical results provide a novel understanding of the performance of ADMM in the presence of nonsmoothness and nonconvexity in the objective functions, through the lens of a restricted strong convexity property. A key nonconvex application of this algorithm is the CT image reconstruction problem, where many interesting open questions remain. In particular, for real CT scanner data, it is important to calibrate the beam intensity and detector sensitivity parameters that characterize the performance of the detector. In future work, we aim to extend the ADMM formulation of the image reconstruction problem to allow for simultaneous estimation of the calibration parameters (a preliminary study of the simultaneous estimation approach can be found in Ha et al. [2018]). From the theoretical perspective, a key remaining question is whether the RSC property can be further relaxed, or whether this condition is necessary for convergence to be guaranteed.

Acknowledgements

R.F.B. and E.Y.S. were both supported by the National Institutes of Health via grant NIH R01-023968. R.F.B. was supported by the National Science Foundation via grant DMS-1654076, and by the Office of Naval Research via grant N00014-20-1-2337. E.Y.S. was supported by National Institutes of Health via grant NIH R01-026282.

References

- Rina Foygel Barber and Emil Y Sidky. MOCCA: Mirrored convex/concave optimization for nonconvex composite functions. *The Journal of Machine Learning Research*, 17(1):5006–5056, 2016.
- Rina Foygel Barber, Emil Y Sidky, Taly Gilat Schmidt, and Xiaochuan Pan. An algorithm for constrained one-step inversion of spectral CT data. *Physics in Medicine & Biology*, 61(10):3784–3818, 2016.
- Alexandre Belloni and Victor Chernozhukov. ℓ_1 -penalized quantile regression in high-dimensional sparse models. *The Annals of Statistics*, 39(1):82–130, 2011.
- Stephen Boyd, Neal Parikh, Eric Chu, Borja Peleato, and Jonathan Eckstein. Distributed optimization and statistical learning via the alternating direction method of multipliers. *Foundations and Trends® in Machine learning*, 3(1):1–122, 2011.

- Antonin Chambolle and Thomas Pock. A first-order primal-dual algorithm for convex problems with applications to imaging. *Journal of mathematical imaging and vision*, 40(1):120–145, 2011.
- Gong Chen and Marc Teboulle. A proximal-based decomposition method for convex minimization problems. *Mathematical Programming*, 64(1-3):81–101, 1994.
- Ethan R Elenberg, Rajiv Khanna, Alexandros G Dimakis, and Sahand Negahban. Restricted strong convexity implies weak submodularity. *The Annals of Statistics*, 46(6B):3539–3568, 2018.
- Suriya Gunasekar, Arindam Banerjee, and Joydeep Ghosh. Unified view of matrix completion under general structural constraints. In *Advances in Neural Information Processing Systems*, pages 1180–1188, 2015.
- Wooseok Ha, Emil Y Sidky, Rina Foygel Barber, Taly Gilat Schmidt, and Xiaochuan Pan. Alternating minimization based framework for simultaneous spectral calibration and image reconstruction in spectral ct. In *2018 IEEE Nuclear Science Symposium and Medical Imaging Conference Proceedings (NSS/MIC)*, pages 1–5. IEEE, 2018.
- Bingsheng He and Xiaoming Yuan. Convergence analysis of primal-dual algorithms for a saddle-point problem: from contraction perspective. *SIAM Journal on Imaging Sciences*, 5(1):119–149, 2012.
- Mingyi Hong, Zhi-Quan Luo, and Meisam Razaviyayn. Convergence analysis of alternating direction method of multipliers for a family of nonconvex problems. *SIAM Journal on Optimization*, 26(1):337–364, 2016.
- Prateek Jain, Ambuj Tewari, and Purushottam Kar. On iterative hard thresholding methods for high-dimensional m-estimation. In *Advances in Neural Information Processing Systems*, pages 685–693, 2014.
- Bo Jiang, Tianyi Lin, Shiqian Ma, and Shuzhong Zhang. Structured nonconvex and nonsmooth optimization: algorithms and iteration complexity analysis. *Computational Optimization and Applications*, 72(1):115–157, 2019.
- Alessandro Lanza, Serena Morigi, Ivan Selesnick, and Fiorella Sgallari. Nonconvex nonsmooth optimization via convex–nonconvex majorization–minimization. *Numerische Mathematik*, 136(2):343–381, 2017.
- Po-Ling Loh and Martin J Wainwright. Regularized m-estimators with nonconvexity: Statistical and algorithmic theory for local optima. *The Journal of Machine Learning Research*, 16(1):559–616, 2015.
- Sindri Magnússon, Pradeep Chathuranga Weeraddana, Michael G Rabbat, and Carlo Fischione. On the convergence of alternating direction lagrangian methods for nonconvex structured optimization problems. *IEEE Transactions on Control of Network Systems*, 3(3):296–309, 2015.

- Mahesh Chandra Mukkamala, Peter Ochs, Thomas Pock, and Shoham Sabach. Convex-concave backtracking for inertial bregman proximal gradient algorithms in non-convex optimization. *arXiv preprint arXiv:1904.03537*, 2019.
- Sahand N Negahban, Pradeep Ravikumar, Martin J Wainwright, and Bin Yu. A unified framework for high-dimensional analysis of m -estimators with decomposable regularizers. *Statistical Science*, 27(4):538–557, 2012.
- Hung Nien and Jeffrey A Fessler. Fast x-ray ct image reconstruction using a linearized augmented lagrangian method with ordered subsets. *IEEE transactions on medical imaging*, 34(2):388–399, 2014.
- Peter Ochs, Alexey Dosovitskiy, Thomas Brox, and Thomas Pock. On iteratively reweighted algorithms for nonsmooth nonconvex optimization in computer vision. *SIAM Journal on Imaging Sciences*, 8(1):331–372, 2015.
- Thomas Pock and Antonin Chambolle. Diagonal preconditioning for first order primal-dual algorithms in convex optimization. In *2011 International Conference on Computer Vision*, pages 1762–1769. IEEE, 2011.
- Taly Gilat Schmidt, Rina Foygel Barber, and Emil Y Sidky. A spectral ct method to directly estimate basis material maps from experimental photon-counting data. *IEEE transactions on medical imaging*, 36(9):1808–1819, 2017.
- Taly Gilat Schmidt, Rina Foygel Barber, and Emil Y Sidky. Spectral ct metal artifact reduction using weighted masking and a one step direct inversion reconstruction algorithm. In *Medical Imaging 2020: Physics of Medical Imaging*, volume 11312, page 113121F. International Society for Optics and Photonics, 2020.
- Emil Y Sidky, Rina Foygel Barber, Taly Gilat-Schmidt, and Xiaochuan Pan. Three material decomposition for spectral computed tomography enabled by block-diagonal step-preconditioning. *arXiv preprint arXiv:1801.06263*, 2018.
- Vidyashankar Sivakumar and Arindam Banerjee. High-dimensional structured quantile regression. In *Proceedings of the 34th International Conference on Machine Learning-Volume 70*, pages 3220–3229. JMLR. org, 2017.
- Tuomo Valkonen. A primal–dual hybrid gradient method for nonlinear operators with applications to mri. *Inverse Problems*, 30(5):055012, 2014.
- Fenghui Wang, Zongben Xu, and Hong-Kun Xu. Convergence of bregman alternating direction method with multipliers for nonconvex composite problems. *arXiv preprint arXiv:1410.8625*, 2014.
- Fenghui Wang, Wenfei Cao, and Zongben Xu. Convergence of multi-block bregman admm for nonconvex composite problems. *Science China Information Sciences*, 61(12):122101, 2018.
- Yu Wang, Wotao Yin, and Jinshan Zeng. Global convergence of admm in nonconvex nonsmooth optimization. *Journal of Scientific Computing*, 78(1):29–63, 2019.

A Additional proofs and calculations

A.1 Completing the proof of Theorem 1

To complete the proof of Theorem 1, we only need to prove that the bound (9) holds under the assumption (8) on the step size matrices H_f, H_g , for any point (x, y, u) with $Ax + By = c$. For the subgradients at the iterations, applying the definitions of x_{t+1} and u_{t+1} we can see that

$$\begin{aligned} 0 &\in \partial f_c(x_{t+1}) + \nabla f_d(x_t) + A^\top u_t + A^\top \Sigma(Ax_{t+1} + By_t - c) + H_f(x_{t+1} - x_t) \\ &= \partial f_c(x_{t+1}) + \nabla f_d(x_t) + A^\top u_{t+1} + H_f(x_{t+1} - x_t), \end{aligned}$$

since $u_{t+1} = u_t + \Sigma(Ax_{t+1} + By_t - c)$. Since $\partial f(x_{t+1}) = \partial f_c(x_{t+1}) + \nabla f_d(x_{t+1})$, this implies

$$\begin{aligned} \langle x_{t+1} - x, \partial f(x_{t+1}) + A^\top u \rangle &= -\langle A(x_{t+1} - x), u_{t+1} - u \rangle \\ &\quad + \langle x_{t+1} - x, \nabla f_d(x_{t+1}) - \nabla f_d(x_t) - H_f(x_{t+1} - x_t) \rangle \end{aligned}$$

where, abusing notation, if the subgradient $\partial f(x_{t+1})$ is not unique then we interpret this expression to mean that the equation holds for *some* choice of the subgradient. We can similarly calculate

$$\begin{aligned} 0 &\in \partial g_c(y_{t+1}) + \nabla g_d(y_t) + B^\top u_{t+1} + B^\top \Sigma(Ax_{t+1} + By_{t+1} - c) + H_g(y_{t+1} - y_t) \\ &= \partial g_c(y_{t+1}) + \nabla g_d(y_t) + B^\top (2u_{t+1} - u_t) + B^\top \Sigma B(y_{t+1} - y_t) + H_g(y_{t+1} - y_t), \end{aligned}$$

and so

$$\begin{aligned} \langle y_{t+1} - y, \partial g(y_{t+1}) + B^\top u \rangle &= \langle y_{t+1} - y, -B^\top (2u_{t+1} - u_t - u) - B^\top \Sigma B(y_{t+1} - y_t) \rangle \\ &\quad + \langle y_{t+1} - y, \nabla g_d(y_{t+1}) - \nabla g_d(y_t) - H_g(y_{t+1} - y_t) \rangle. \end{aligned}$$

Since $Ax + By = c$ by assumption, and $u_{t+1} = u_t + \Sigma(Ax_{t+1} + By_t - c)$ by definition, we can further calculate

$$\begin{aligned} &\langle y_{t+1} - y, -B^\top (2u_{t+1} - u_t - u) - B^\top \Sigma B(y_{t+1} - y_t) \rangle \\ &= \begin{pmatrix} y_{t+1} - y \\ u_{t+1} - u \end{pmatrix}^\top \begin{pmatrix} B^\top \Sigma B & B^\top \\ B & \Sigma^{-1} \end{pmatrix} \begin{pmatrix} y_t - y_{t+1} \\ u_t - u_{t+1} \end{pmatrix} - \langle \Sigma^{-1}(u_t - u_{t+1}) + B(y_t - y), u_{t+1} - u \rangle \\ &= \begin{pmatrix} y_{t+1} - y \\ u_{t+1} - u \end{pmatrix}^\top \begin{pmatrix} B^\top \Sigma B & B^\top \\ B & \Sigma^{-1} \end{pmatrix} \begin{pmatrix} y_t - y_{t+1} \\ u_t - u_{t+1} \end{pmatrix} + \langle A(x_{t+1} - x), u_{t+1} - u \rangle. \end{aligned}$$

Combining our calculations so far, we have

$$\begin{aligned} \left\langle \begin{pmatrix} x_{t+1} - x \\ y_{t+1} - y \end{pmatrix}, \begin{pmatrix} \partial f(x_{t+1}) + A^\top u \\ \partial g(y_{t+1}) + B^\top u \end{pmatrix} \right\rangle &= (z_{t+1} - z)^\top M(z_t - z_{t+1}) \\ &\quad + \langle x_{t+1} - x, \nabla f_d(x_{t+1}) - \nabla f_d(x_t) \rangle + \langle y_{t+1} - y, \nabla g_d(y_{t+1}) - \nabla g_d(y_t) \rangle, \quad (18) \end{aligned}$$

where we define $z = (x, y, u)$ and $z_t = (x_t, y_t, u_t)$ for each t , and let

$$M = \begin{pmatrix} H_f & 0 & 0 \\ 0 & H_g + B^\top \Sigma B & B^\top \\ 0 & B & \Sigma^{-1} \end{pmatrix} \succeq 0.$$

Next, defining $\|v\|_M = \sqrt{v^\top M v}$, we can use a telescoping sum to calculate

$$\begin{aligned} \sum_{t=0}^{T-1} (z_{t+1} - z)^\top M (z_t - z_{t+1}) &= \sum_{t=0}^{T-1} \left(\frac{1}{2} \|z - z_t\|_M^2 - \frac{1}{2} \|z - z_{t+1}\|_M^2 - \frac{1}{2} \|z_t - z_{t+1}\|_M^2 \right) \\ &= \frac{1}{2} \|z - z_0\|_M^2 - \frac{1}{2} \|z - z_T\|_M^2 - \frac{1}{2} \sum_{t=0}^{T-1} \|z_t - z_{t+1}\|_M^2. \end{aligned}$$

Furthermore,

$$\begin{aligned} \|z_t - z_{t+1}\|_M^2 &= \|x_t - x_{t+1}\|_{H_f}^2 - \|y_t - y_{t+1}\|_{H_g}^2 \\ &= \begin{pmatrix} y_t - y_{t+1} \\ u_t - u_{t+1} \end{pmatrix}^\top \begin{pmatrix} B^\top \Sigma B & B^\top \\ B & \Sigma^{-1} \end{pmatrix} \begin{pmatrix} y_t - y_{t+1} \\ u_t - u_{t+1} \end{pmatrix} \\ &= \|\Sigma^{-1}(u_t - u_{t+1}) + B(y_t - y_{t+1})\|_\Sigma^2 = \|Ax_{t+1} + By_{t+1} - c\|_\Sigma^2, \end{aligned}$$

where the last step plugs in the update step for u_{t+1} . Combining these calculations with (18), we obtain

$$\begin{aligned} &\sum_{t=0}^{T-1} \left\langle \begin{pmatrix} x_{t+1} - x \\ y_{t+1} - y \end{pmatrix}, \begin{pmatrix} \partial f(x_{t+1}) + A^\top u \\ \partial g(y_{t+1}) + B^\top u \end{pmatrix} \right\rangle \\ &= \frac{1}{2} \|z - z_0\|_M^2 - \frac{1}{2} \|z - z_T\|_M^2 - \frac{1}{2} \sum_{t=0}^{T-1} \|Ax_{t+1} + By_{t+1} - c\|_\Sigma^2 \\ &\quad + \sum_{t=0}^{T-1} \left[\langle x_{t+1} - x, \nabla f_d(x_{t+1}) - \nabla f_d(x_t) \rangle - \frac{1}{2} \|x_t - x_{t+1}\|_{H_f}^2 \right] \\ &\quad + \sum_{t=0}^{T-1} \left[\langle y_{t+1} - y, \nabla g_d(y_{t+1}) - \nabla g_d(y_t) \rangle - \frac{1}{2} \|y_t - y_{t+1}\|_{H_g}^2 \right]. \quad (19) \end{aligned}$$

Now, since $H_f \succeq \nabla^2 f_d(x)$, we can write

$$f_d(x_{t+1}) \leq f_d(x_t) + \langle x_{t+1} - x_t, \nabla f_d(x_t) \rangle + \frac{1}{2} \|x_t - x_{t+1}\|_{H_f}^2$$

for each t . Rearranging terms and taking a telescoping sum, this means that

$$\begin{aligned} &\sum_{t=0}^{T-1} \left[\langle x_{t+1} - x, \nabla f_d(x_{t+1}) - \nabla f_d(x_t) \rangle - \frac{1}{2} \|x_t - x_{t+1}\|_{H_f}^2 \right] \\ &\leq f_d(x_0) - f_d(x_T) + \langle x - x_0, \nabla f_d(x_0) \rangle - \langle x - x_T, \nabla f_d(x_T) \rangle. \end{aligned}$$

Again applying $H_f \succeq \nabla^2 f_d(x)$, we also have

$$f_d(x) \leq f_d(x_T) + \langle x - x_T, \nabla f_d(x_T) \rangle + \frac{1}{2} \|x - x_T\|_{H_f}^2$$

and

$$f_d(x_0) \leq f_d(x) + \langle x_0 - x, \nabla f_d(x) \rangle + \frac{1}{2} \|x - x_0\|_{H_f}^2,$$

which combined with the above yields

$$\begin{aligned} & \sum_{t=0}^{T-1} \left[\langle x_{t+1} - x, \nabla f_d(x_{t+1}) - \nabla f_d(x_t) \rangle - \frac{1}{2} \|x_t - x_{t+1}\|_{H_f}^2 \right] \\ & \leq -\langle x - x_0, \nabla f_d(x) - \nabla f_d(x_0) \rangle + \frac{1}{2} \|x - x_T\|_{H_f}^2 + \frac{1}{2} \|x - x_0\|_{H_f}^2. \end{aligned}$$

Performing an identical calculation for the y terms, and combining these calculations with (19) along with the fact that $\|z - z_T\|_M^2 \geq \|x - x_T\|_{H_f}^2 + \|y - y_T\|_{H_g}^2$, we obtain

$$\begin{aligned} & \sum_{t=0}^{T-1} \left\langle \begin{pmatrix} x_{t+1} - x \\ y_{t+1} - y \end{pmatrix}, \begin{pmatrix} \partial f(x_{t+1}) + A^\top u \\ \partial g(y_{t+1}) + B^\top u \end{pmatrix} \right\rangle \\ & \leq C(x, y, u; x_0, y_0, u_0) - \frac{1}{2} \sum_{t=0}^{T-1} \|Ax_{t+1} + By_{t+1} - c\|_\Sigma^2, \end{aligned}$$

where we define

$$\begin{aligned} C(x, y, u; x_0, y_0, u_0) &= \frac{1}{2} \|z - z_0\|_M^2 - \langle x - x_0, \nabla f_d(x) - \nabla f_d(x_0) \rangle + \frac{1}{2} \|x - x_0\|_{H_f}^2 \\ & \quad - \langle y - y_0, \nabla g_d(y) - \nabla g_d(y_0) \rangle + \frac{1}{2} \|y - y_0\|_{H_g}^2. \end{aligned} \quad (20)$$

This proves the desired bound (9), and verifies that

$$C(x, y, u; x_0, y_0, u_0) = \mathcal{O}(\|(x, y, u) - (x_0, y_0, u_0)\|_2^2)$$

in the case that f_d and g_d have Lipschitz gradients.

A.2 Details for the sparse quantile regression example

We now compute the steps of Algorithm 1 for the sparse quantile regression example, i.e., for the problem of minimizing (10). Plugging in our choices of the parameters H_f, H_g, Σ and of A, B, c , the steps of Algorithm 1 are given by

$$\begin{aligned} x_{t+1} &= \arg \min_{x \in \mathbb{R}^d} \left\{ f_c(x) + \langle \nabla f_d(x_t), x \rangle + \langle u_t, \Phi x \rangle + \frac{\sigma}{2} \|\Phi x - y_t\|_2^2 + \frac{\sigma}{2} \|x - x_t\|_{\gamma \mathbf{I}_d - \Phi^\top \Phi}^2 \right\}, \\ u_{t+1} &= u_t + \sigma(\Phi x_{t+1} - y_t), \\ y_{t+1} &= \arg \min_{y \in \mathbb{R}^n} \left\{ g_c(y) + \langle \nabla g_d(y_t), y \rangle - \langle u_{t+1}, y \rangle + \frac{\sigma}{2} \|\Phi x_{t+1} - y\|_2^2 \right\}. \end{aligned}$$

Now we compute the x and y update steps explicitly. First, for x , recall that $f_c(x) = \lambda \sum_{j=1}^d |x_j|$ and

$$f_d(x) = \lambda \sum_{j=1}^d (\beta \log(1 + |x_j|/\beta) - |x_j|).$$

We can calculate the gradient as

$$[\nabla f_d(x)]_j = -\frac{\lambda x_j}{\beta + |x_j|}.$$

By our choice of $H_f = \sigma(\gamma \mathbf{I}_d - \Phi^\top \Phi)$, we see that the x update step separates over the d entries of x :

$$\begin{aligned} f_c(x) + \langle \nabla f_d(x_t), x \rangle + \langle u_t, \Phi x \rangle + \frac{\sigma}{2} \|\Phi x - y_t\|_2^2 + \frac{\sigma}{2} \|x - x_t\|_{\gamma \mathbf{I}_d - \Phi^\top \Phi}^2 \\ = \sum_{j=1}^d \left(\lambda |x_j| + \frac{\sigma \gamma}{2} x_j^2 - x_j \cdot \left[\frac{\lambda (x_t)_j}{\beta + |(x_t)_j|} + \sigma(\gamma x_t - \Phi^\top (\Phi x_t - y_t + u_t/\sigma))_j \right] \right). \end{aligned}$$

This is minimized by setting x_{t+1} to have entries

$$(x_{t+1})_j = \text{SoftThresh}_{\frac{\lambda}{\sigma \gamma}} \left((x_t)_j - \frac{(\Phi^\top (\Phi x_t - y_t + u_t/\sigma))_j}{\sigma \gamma} + \frac{\lambda}{\sigma \gamma} \cdot \frac{(x_t)_j}{\beta + |(x_t)_j|} \right),$$

where the soft thresholding function is defined as

$$\text{SoftThresh}_\lambda(t) = \begin{cases} t - \lambda, & \text{if } t > \lambda, \\ 0, & \text{if } |t| \leq \lambda, \\ t + \lambda, & \text{if } t < -\lambda. \end{cases}$$

Next, for the y update step, recall $g_d(y) \equiv 0$ and

$$g_c(y) = \sum_{i=1}^n q \max\{w_i - y_i, 0\} + (1 - q) \max\{y_i - w_i, 0\}.$$

Then the optimization problem for the y update step also separates over the n entries of y :

$$\begin{aligned} g_c(y) + \langle \nabla g_d(y_t), y \rangle - \langle u_{t+1}, y \rangle + \frac{\sigma}{2} \|\Phi x_{t+1} - y\|_2^2 \\ = \sum_{i=1}^n \left(q \max\{w_i - y_i, 0\} + (1 - q) \max\{y_i - w_i, 0\} + \frac{\sigma}{2} y_i^2 - y_i \cdot (\sigma(\Phi x_{t+1})_i + (u_{t+1})_i) \right). \end{aligned}$$

This is minimized by setting y_{t+1} to have entries

$$(y_{t+1})_i = \begin{cases} (\Phi x_{t+1})_i + \frac{(u_{t+1})_i}{\sigma} + \frac{q}{\sigma}, & \text{if } (\Phi x_{t+1})_i + \frac{(u_{t+1})_i}{\sigma} + \frac{q}{\sigma} < w_i, \\ (\Phi x_{t+1})_i + \frac{(u_{t+1})_i}{\sigma} - \frac{1-q}{\sigma}, & \text{if } (\Phi x_{t+1})_i + \frac{(u_{t+1})_i}{\sigma} - \frac{1-q}{\sigma} > w_i, \\ w_i, & \text{if } (\Phi x_{t+1})_i + \frac{(u_{t+1})_i}{\sigma} - \frac{1-q}{\sigma} \leq w_i \leq (\Phi x_{t+1})_i + \frac{(u_{t+1})_i}{\sigma} + \frac{q}{\sigma}. \end{cases}$$

A.3 Details for the CT application

To run Algorithm 1 for the CT image reconstruction problem 16, plugging in our choices of parameters H_f, H_g, Σ and the values of A, B, c and $f(x) \equiv 0$, our update steps are:

$$\begin{cases} x_{t+1} = x_t + Q_f^{-1} P^\top (\Sigma(y_t - Px_t) - u_t), \\ u_{t+1} = u_t + \Sigma(Px_{t+1} - y_t), \\ y_{t+1} = \arg \min_y \{g_c(y) + y^\top \nabla g_d(y_t) + \frac{1}{2} y^\top \Sigma y - y^\top (u_{t+1} + \Sigma Px_{t+1})\}. \end{cases} \quad (21)$$

Now we examine the calculations required for these update steps:

- Since Q_f and Σ are diagonal while P is sparse, the x and u update steps require only inexpensive matrix-vector calculations.
- For the y update step, we will use the Newton–Raphson method to solve the minimization subproblem approximately: setting $y_{t+1}^{(0)} = y_t$, we define

$$y_{t+1}^{(i+1)} = y_{t+1}^{(i)} - (\nabla^2 g_c(y_{t+1}^{(i)}) + \Sigma)^{-1} \left(\nabla g_c(y_{t+1}^{(i)}) + \nabla g_d(y_t) + \Sigma(y_{t+1}^{(i)} - Px_{t+1}) - u_{t+1} \right),$$

for each $i = 0, 1, 2, \dots, N - 1$, and then set $y_{t+1} = y_{t+1}^{(N)}$. While each step of Newton–Raphson appears to require the inversion of a $n_\ell n_m \times n_\ell n_m$ matrix, in fact this calculation is very simple since Σ is diagonal while $\nabla^2 g_c(y_{t+1}^{(i)})$ is block-diagonal, with n_ℓ many $n_m \times n_m$ blocks (this is because $g_c(y)$ separates over the rays $\ell = 1, \dots, n_\ell$, as defined in (17)). Since we typically work with a small number of materials (e.g., $n_m = 3$ or $n_m = 5$), solving each one of convex minimization problems is computationally very inexpensive. In our implementation, at each iteration t we run $N = 10$ steps of the Newton–Raphson method to compute the y update, which is sufficient to obtain a near-exact solution.